Mechanisms Underlying a Quantum Superposition Microscope Based on THz-Driven Coherent Oscillations in a Two-Level Molecular Sensor

Yunpeng Xia[●],[1] Likun Wang[●],[1] and W. Ho[●][1,2,*]

[1]*Department of Physics and Astronomy, University of California, Irvine, California 92697-4575, USA*
[2]*Department of Chemistry, University of California, Irvine, California 92697-2025, USA*

We report pump-probe measurements of a hydrogen molecule (H_2) in the tunnel junction of a scanning tunneling microscope coupled to ultrashort terahertz (THz) pulses. The coherent oscillation of the THz-induced dc tunneling current at a frequency of ∼0.5 THz fingerprints the absorption by H_2 as a two-level system (TLS). Two components of the oscillatory signal are observed and point to both photon and field aspects of the THz pulses. A few loosely bound states with similar energies for the upper state of the TLS are evidenced by the coherent revival of oscillatory signal. Furthermore, the comparison of spectroscopic features of H_2 with different tips provides an understanding of the TLS for H_2.

The trapping modes for H_2 weakly adsorbed on noble metal surfaces or within cavities have energies comparable to the weak Van der Waals interaction [1,2]. The diffusive nature of adsorbed H_2 on surfaces adds to the challenge of reaching a definitive determination of the properties of these modes. Nevertheless, previous studies have implied the connections of these low-energy modes to several fundamental phenomena, including negative differential resistance (NDR) [3–6], stochastic resonance [7], zero-bias anomaly [8], enhanced imaging ability [8–11] and charge transfer as an electron donor [12]. A double-well two-level system (TLS) consisting of the ground state and one other low-energy trapping state could explain these phenomena of H_2 in the tunnel junction [4,7]. The potential use of H_2 as an atomic-scale sensor demands a comprehensive understanding of the energy profile and response of the TLS to the local environment within the tunnel junction.

Extreme spatial and temporal resolutions have been achieved by pump-probe measurements combining ultrashort THz pulses with the scanning tunneling microscope (STM) [13–16]. Behaving as an ultrafast yet quasistatic alternating bias, THz pulses not only coherently control the electron tunneling across the junction and affect the associated dynamics [17], but also have tolerable thermal effects on the junction stability, which enables the study of action spectroscopy of single molecules [13–15].

In this Letter, we report the direct observation of Ramsey fringes arising from transitions between two close-lying states of H_2 with a THz-STM setup of the quantum superposition microscope (QSM) [18]. The polarization of THz pulses is parallel to the tip axis, and the calibrated THz-induced voltage in the STM junction is ∼10 mV [18]. A topographic image of the single layer island of Cu_2N is shown in Fig. 1(a). The H_2 behaved as a 3D rotor, exhibiting a rotational excitation spectrum that could

be used to fingerprint and indicate the concentration of H_2 [10,36–38]. We performed both inelastic electron tunneling spectroscopy (IETS) and single beam THz-induced dc current spectroscopy (TIDCS) over the same position of Cu_2N [Fig. 1(b)]. The two measurements should, in principle, exhibit similar spectra related to the d^2I/dV^2 of the junction. The IETS showed a broad bouncing vibration mode from 10 to 30 mV, with $j = 0 \rightarrow 2$ rotational excitation from 40 to 60 mV [10,11,25,36–38], and one low-energy excitation from 0 to 10 mV whose origin is still under debate [8]. However, the TIDCS differed in having a feature of opposite curvature spanning from 10 to 40 mV and in the line shape for the rotational excitation. Although the change from peak dip to Gaussian line shape of the rotational mode agrees with the theory of the frequency response of a driven double-well system [39], the experimental observation combined with the simulation detailed in Ref. [18] indicated that the additional light-matter interaction was not associated with the nonsinusoidal bias modulation induced by the THz pulses in the junction, unlike previous THz rectification spectroscopy [13,40–42].

To analyze the effect of THz irradiation on the dynamics of H_2 on Cu_2N in the STM junction, we measured the dc current induced by pump-probe THz pulses. The coherent oscillations in the dc current as a function of the time delay τ are shown in Fig. 1(c), and Fast Fourier Transform (FFT) reveals frequencies below 1 THz (4.14 meV) [Fig. 1(d)]. The phonon excitation energies of an H_2 cluster are in the range of 5 to 10 meV [38,43]. The energy splitting of degenerate excited rotational levels due to perturbation from the local environment can be below 4 meV [25]. However, occupation of the lowest excited rotational state is negligible to allow transitions between split levels. Low-lying trapping states
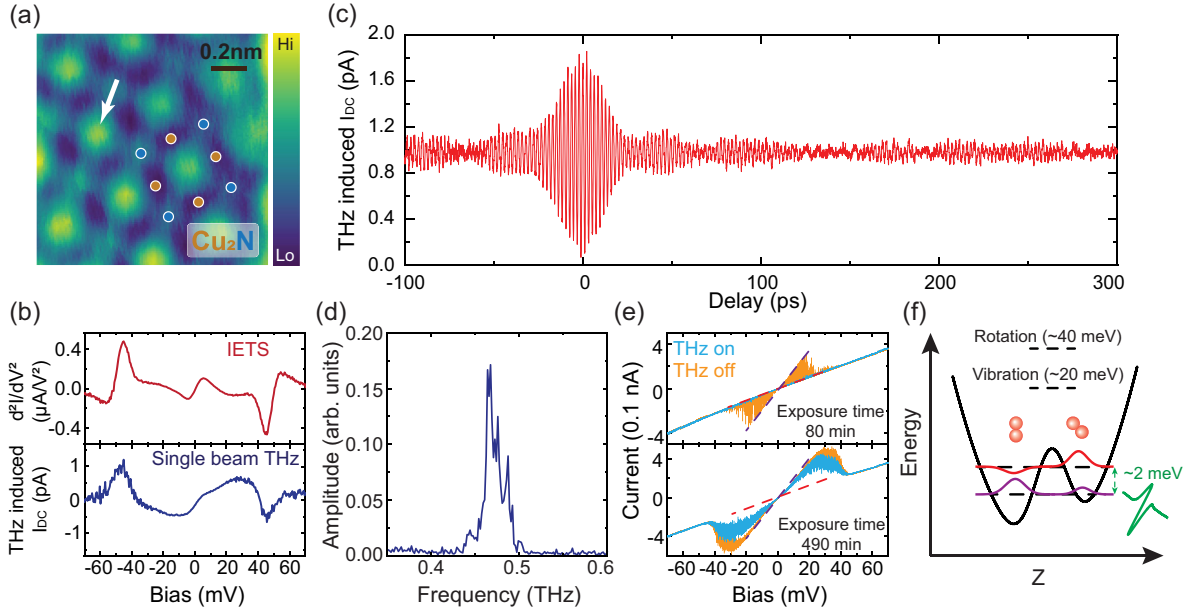
FIG. 1. Spectroscopic fingerprints of H_2 (a) Constant current topographic image of a Cu_2N surface with setpoint -20 mV/40 pA. (b) IETS spectrum (3 mV modulation at 263.03 Hz) and chopped single beam TIDCS taken at the same spot marked by the white arrow in (a), with the same setpoint -20 mV/40 pA. (c) The pump-probe delay scan of the THz-induced dc current with tip bias ramped to $+20$ mV after turning off the feedback at setpoint -20 mV/40 pA. (d) FFT spectrum of (c). (e) I-V spectra taken over Cu_2N surface with and without THz irradiation with setpoint 100 mV/500 pA for low and high concentrations of H_2. The dashed purple (red) line corresponds to the I-V curve for the high (low) conductance state. (f) Schematic diagram of the tilted double-well potential and two possible H_2 configurations. The tip used here belongs to type II mentioned in Fig. 3.

have been used to describe a single hydrogen molecule in a nanocavity [4,7]. The existence of these modes was indicated by the switching in the I-V spectra in Fig. 1(e). The distinct conductance levels corresponded to different adsorption states in a double-well potential as illustrated in Fig. 1(f). The switching events near zero bias suggested a small separation in energy between the two states. The effect of THz pulses on the TLS of H_2 could be further examined by varying the exposure time of background H_2 in the chamber. The THz pulses were seen to suppress the switching by restraining the H_2 to a low conductance state at a low concentration of H_2, while the high conductance state became the ground state in the bias range from -30 to 30 mV at a high concentration of H_2. The I-V spectrum under THz irradiation indicated a shift of H_2 to the low conductance state as evidenced by a decrease in the magnitude of current, like the trend observed in the low concentration case.

Given the resonant absorption of THz photons by H_2 molecules, we show in Fig. 2(a) that the induced dc current $I_{DC}(V_{DC}, \tau)$ from the THz pump-probe pulses should contain two parts [18], which is like the signal decomposition in [44],

$$I_{DC}(V_{DC}, \tau) = I_s(V_{DC}, \tau) + I_d(V_{DC}, \tau). \quad (1)$$

$I_s(V_{DC}, \tau)$ is the rectified current of the STM junction with nonlinear I-V characteristics, modulated by ac voltage from two interfering postabsorption THz pulses, while

$I_d(V_{DC}, \tau)$ is the elastic tunneling current driven by the dc sample bias, measuring the conductance oscillations $\sigma_{osc}(\tau)$ due to the population change in the TLS of H_2 induced by THz photons. Elaborated by a model based on the Ramsey fringe of the TLS for H_2, we show in Ref. [18] that

$$I_d(V_{DC}, \tau) \propto \sigma_{osc}(\tau) = \frac{(\sigma_{11} - \sigma_{22})\sin^2\alpha e^{-\gamma\tau}\cos\omega\tau}{2}, \quad (2)$$

where $\sigma_{11(22)}$ represents the conductance of the two states of H_2, α for simplicity of analysis the assumed rotational angle induced by each THz pulse in the Bloch sphere, γ the transverse decay rate, and $\hbar\omega = \varepsilon_2 - \varepsilon_1$ the energy difference of the two levels. The variation of I_s and I_d during the pump-probe cycles is also shown in Fig. 2(b). In Fig. 2(c), the FFT spectrum of $I_s(V_{DC}, \tau)$ features a sharp absorption dip on the broadband background from THz-induced near field in the junction. The resonant photons are absorbed while the other frequency components from THz field still contribute to the rectification current. In comparison, $I_d(V_{DC}, \tau)$ exhibits a Lorentzian peak in the frequency domain. As shown in Ref. [18], the existence of both components is necessary to reconstruct the oscillatory signal as their contributions to the signal vary at different delays. $I_s(V_{DC}, \tau)$ dominates in the zero-delay-peak region where the two pulses overlap and the oscillation at longer delay time for its larger decay constant, while $I_d(V_{DC}, \tau)$ prevails in the other range.
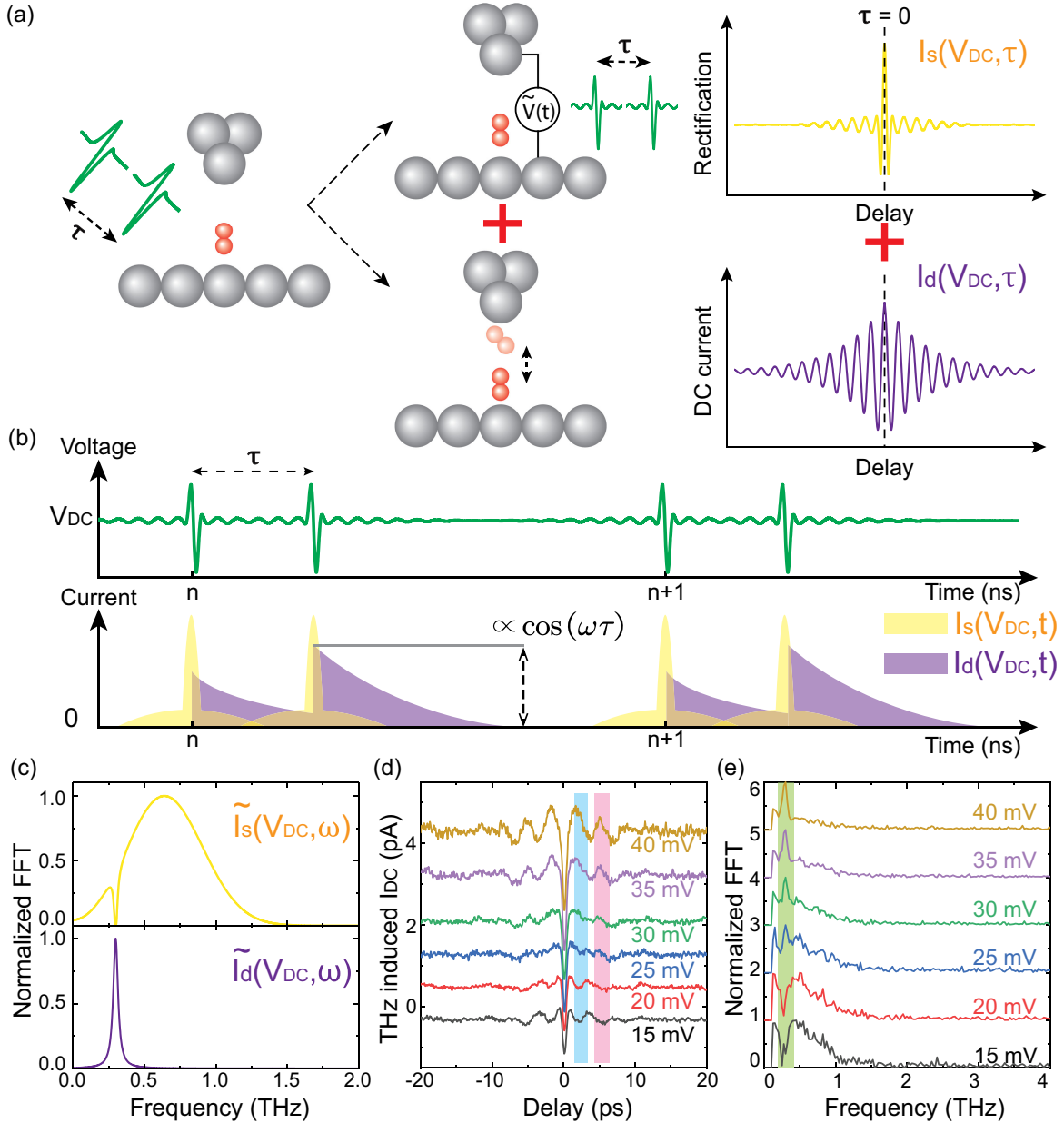
FIG. 2. Absorption and excitation. (a) A schematic diagram showing the two components, $I_s(V_{DC}, \tau)$ and $I_d(V_{DC}, \tau)$, that contribute to an oscillatory delay-scan signal of THz-induced dc current. The resonance frequency of H_2 is set as 0.3 THz with 20 GHz intrinsic broadening. (b) The variation of $I_s(V_{DC}, \tau)$ and $I_d(V_{DC}, \tau)$ in each pump-probe cycle. (c) The FFT spectra of $I_s(V_{DC}, \tau)$ and $I_d(V_{DC}, \tau)$. (d) The delay-scan spectra of H_2 for another tip at different sample biases. The tip located at the same lattice site as Fig. 1(a) and tip height was set by the same setpoint -20 mV/40 pA. (e) The corresponding FFT spectra of (d); the gap below 0.1 THz is the result of a 0.1 THz high-pass filter used in data processing (Sec. I of the Supplemental Material). The tip used here belongs to type I mentioned in Fig. 3.

The competition of the two components was even observed at a certain range of sample bias for a different tip in Figs. 2(d) and 2(e), where the transition from $I_s(V_{DC}, \tau)$ to $I_d(V_{DC}, \tau)$ is accompanied by the dip-to-peak transition at the resonance frequency of H_2 [Fig. 2(e)]. The oscillation feature of $I_s(V_{DC}, \tau)$ highlighted by the blue shaded area vanished with the increasing sample bias, accompanied by the emerging feature of $I_d(V_{DC}, \tau)$ highlighted by the pink shaded rectangle [Fig. 2(d)]. The

broadband background from $I_s(V_{DC}, \tau)$ in Fig. 2(e) differs from the FFT of calculated $I_s(V_{DC}, \tau)$ [top panel of Fig. 2(c)] owing to the low-pass filter effect of the junction [22,45–47], which we did not include in our fitting form. It should be noted that the pure rectified current part, $I_s(V_{DC}, \tau)$, is sufficient to include all the physics for most systems studied by THz-STM [13,40–42], while the elastic tunneling current part, $I_d(V_{DC}, \tau)$, covers a recent work by S. Sheng et al. where THz pulses act as force shaking the

thin Au film [48]. To observe both components simultaneously, a resonant absorption of THz pulses is required, and the lifetime of the excited level should be long enough for the dynamics to be observed in $I_d(V_{DC}, \tau)$.

Two types of the tips showing Ramsey fringes of H_2 but with distinct spectral features were commonly observed in the experiments. At the same setpoint, $I_d(V_{DC}, \tau)$ plays the major role in the delay-scan signal for one type (type II), as for the case of Fig. 1(c), while the other one (type I) is dominated by $I_s(V_{DC}, \tau)$, featured by the pronounced zero-delay peak [16]. Through the IETS at different tip-sample distances in Figs. S12(a) and S12(c), we can determine that the type II tip corresponds to a smaller junction since the IETS at the setpoint -20 mV/40 pA for the type II tip is like the one at the setpoint -20 mV/100 pA for the type I tip. Considering the asymmetrical geometry of the junction, H_2, being an electron blockade, is probably closer to tip in the case of type II, and the resulting functionalized tip is normally accompanied by higher-resolution topography images (results from multiple other tips are provided in Fig. S13). Therefore, a smaller junction for the type II tip, which is more sensitive to conductance fluctuations of H_2, should imply a larger contribution to the delay-scan spectrum from $I_d(V_{DC}, \tau)$ than that of the type I tip. TIDCS relies on the modulation of the evanescent field in the junction induced by THz pulses [20,49]. Compared to electrical modulation used in IETS, the evanescent field is more localized near the tip apex and therefore more sensitive to the relative position of H_2, which could explain the striking discrepancy of TIDCS between the two types of the tip [Figs. S12(b) and S12(d)]. The THz-induced H_2 dynamics should also be more pronounced for the type II tip, as seen in TIDCS where the signal in the NDR region of the vibration mode (15–30 meV) totally changed its sign compared to its IETS. Another substantial observation was that TIDCS for both types of the tip closely resembled its corresponding IETS at a smaller junction, indicating weaker THz-induced dynamics. Moreover, the Ramsey fringes faded away faster at a smaller junction [Fig. S14]. We can thus exclude the possibility that the tunneling electrons assisted by THz radiation are triggering the dynamics. The THz radiation is absorbed by the TLS as photon, and the superposition of ground and excited states are monitored through delay varying elastic tunneling current. These results contrast with single-molecule dynamics excited by THz assisted tunneling electrons which transiently charge the molecule [13–15].

Furthermore, we measured the delay-scan spectrum at different biases to check how the energy spacing of the two levels responds to the external electrical field. Surprisingly, for the type I tip, the resonance frequency always showed a positive slope with respect to the sample bias [Fig. 3(a)], while it showed a negative slope for the type II tip [Fig. 3(b)]. It is known that the Van der Waals force acting on the H_2 induces its dipole moment,
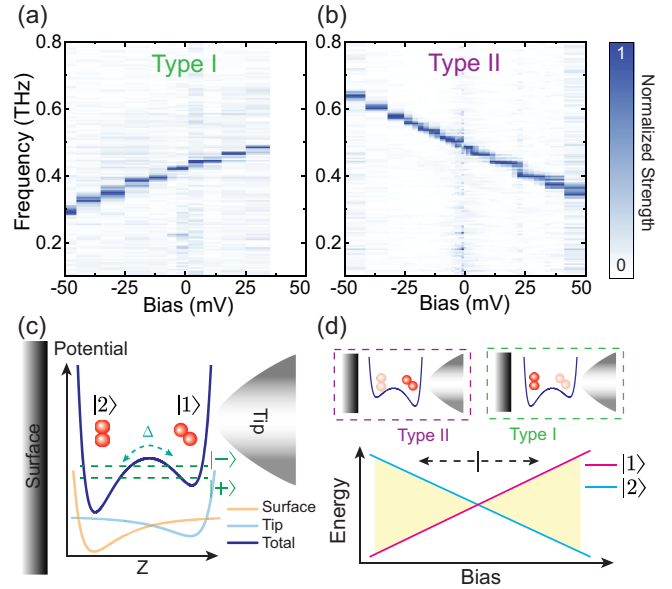

FIG. 3. Bias dependence of single H_2 coherence. (a),(b) The FFT results of the delay scan spectra (-100 ps to 100 ps) for all the biases, acquired at the same tip height set with -20 mV/40 pA and on the same lattice site, with the two types of the tips. (c) The schematic diagram of the TLS for H_2 in a STM junction; the potential landscape is formed by Van der Waals interaction from both tip and sample surface. (d) The schematic diagram shows the double-well potential for the two types of the tip. The bottom panel indicates the linear Stark shift of the two conformational states with respect to sample bias, and the difference between the two lines is the resonance frequency of H_2, observed in delay-scan spectra.

which varies with separation between the H_2 and sample surface [26,50]. The resonance frequency of H_2 shifts since its two states with individual dipole moments respond differently to the electric field. We could thus predict the TLS of H_2 as schematically shown in Fig. 3(c). Owing to Van der Waals interaction, the double-well potential is expected in the geometry of the tunneling junction, where the two minimum occur at the vicinity of the sample surface and tip. Depending on which state is more energetically favorable, we have two types of tips [Fig. 3(d)]. Without including the higher order polarization terms, the energy of the two states linearly depend on the sample bias, and the resonance frequency of the TLS can be schematically represented by the yellow shaded area in Fig. 3(d), which agrees with the bias-dependence data in Figs. 3(a) and 3(b). It should be mentioned that there exists tunneling coupling Δ between the two states of H_2, and therefore the actual eigenstates ($|+\rangle$ and $|-\rangle$) of this system are the superposition of the two conformational states ($|1\rangle$ and $|2\rangle$). Nevertheless, away from the cross region where the energy of $|1\rangle$ and $|2\rangle$ are close, the eigenstates are mostly either $|1\rangle$ or $|2\rangle$, which is the regime that this paper considers. A recent work [51] has demonstrated that, by tuning the sample bias, the ground state of H_2 can be

adiabatically changed from one to another, showing the combined spectral features from the two types of the tip. An additional discussion on the nature of TLS for H_2 can be found in Ref. [18].

In summary, a sub-THz TLS has been discovered for the H_2 molecule within the STM tunnel junction. The origin of the THz-induced dc current in the delay scan has been theoretically analyzed, and the Ramsey fringe of the TLS elucidates the power of the THz-STM based QSM to evaluate potential nanoscale qubits based on molecules. The absorption of THz radiation points to its behavior as photons, while simultaneously its field leads to the rectification current which reflects absorption at the resonance frequency. In addition, the analysis on the spectroscopic fingerprints of H_2 sheds light on the nature of the TLS of H_2 in the junction.

*Corresponding author: wilsonho@uci.edu

[1] P. Avouris, D. Schmeisser, and J. E. Demuth, Observation of rotational excitations of H_2 adsorbed on Ag surfaces, Phys. Rev. Lett. **48**, 199 (1982).

[2] K. Svensson and S. Andersson, Dipole active vibrational motion in the physisorption well, Phys. Rev. Lett. **78**, 2016 (1997).

[3] J. A. Gupta, C. P. Lutz, A. J. Heinrich, and D. M. Eigler, Strongly coverage-dependent excitations of adsorbed molecular hydrogen, Phys. Rev. B **71**, 115416 (2005).

[4] W. H. A. Thijssen, D. Djukic, A. F. Otte, R. H. Bremmer, and J. M. Van, Ruitenbeek, Vibrationally induced two-level systems in single-molecule junctions, Phys. Rev. Lett. **97**, 226806 (2006).

[5] A. Halbritter, P. Makk, S. Csonka, and G. Mihály, Huge negative differential conductance in $Au - H_2$ molecular nanojunctions, Phys. Rev. B **77**, 075402 (2008).

[6] M. L. Trouwborst, E. H. Huisman, S. J. van der Molen, and B. J. van Wees, Bistable hysteresis and resistance switching in hydrogen-gold junctions, Phys. Rev. B **80**, 081407(R) (2009).

[7] C. Lotze, M. Corso, K. J. Franke, F. Von Oppen, and J. I. Pascual, Driving a macroscopic oscillator with the stochastic motion of a hydrogen molecule, Science **338**, 779 (2012).

[8] R. Temirov, S. Soubatch, O. Neucheva, A. C. Lassise, and F. S. Tautz, A novel method achieving ultra-high geometrical resolution in scanning tunnelling microscopy, New J. Phys. **10**, 053012 (2008).

[9] C. Weiss, C. Wagner, C. Kleimann, M. Rohlfing, F. S. Tautz, and R. Temirov, Imaging Pauli repulsion in scanning tunneling microscopy, Phys. Rev. Lett. **105**, 086103 (2010).

[10] S. Li, A. Yu, F. Toledo, Z. Han, H. Wang, H. Y. He, R. Wu, and W. Ho, Rotational and vibrational excitations of a hydrogen molecule trapped within a nanocavity of tunable dimension, Phys. Rev. Lett. **111**, 146102 (2013).

[11] H. Wang, S. Li, H. He, A. Yu, F. Toledo, Z. Han, W. Ho, and R. Wu, Trapping and characterization of a single hydrogen molecule in a continuously tunable nanocavity, J. Phys. Chem. Lett. **6**, 3453 (2015).

[12] S. Li, D. Yuan, A. Yu, G. Czap, R. Wu, and W. Ho, Rotational spectromicroscopy: Imaging the orbital interaction between molecular hydrogen and an adsorbed molecule, Phys. Rev. Lett. **114**, 206101 (2015).

[13] T. L. Cocker, D. Peller, P. Yu, J. Repp, and R. Huber, Tracking the ultrafast motion of a single molecule by femtosecond orbital imaging, Nature (London) **539**, 263 (2016).

[14] D. Peller, L. Z. Kastner, T. Buchner, C. Roelcke, F. Albrecht, N. Moll, R. Huber, and J. Repp, Sub-cycle atomic-scale forces coherently control a single-molecule switch, Nature (London) **585**, 58 (2020).

[15] D. Peller, C. Roelcke, L. Z. Kastner, T. Buchner, A. Neef, J. Hayes, F. Bonafé, D. Sidler, M. Ruggenthaler, A. Rubio, R. Huber, and J. Repp, Quantitative sampling of atomic-scale electromagnetic waveforms, Nat. Photonics **15**, 143 (2021).

[16] L. Wang, Y. Xia, and W. Ho, Atomic-scale quantum sensing based on the ultrafast coherence of an H_2 molecule in an STM cavity, Science **376**, 401 (2022).

[17] K. Yoshioka, I. Katayama, Y. Minami, M. Kitajima, S. Yoshida, H. Shigekawa, and J. Takeda, Real-space coherent manipulation of electrons in a single tunnel junction by single-cycle terahertz electric fields, Nat. Photonics **10**, 762 (2016).

[18] See the Supplemental Material at http://link.aps.org/supplemental/10.1103/PhysRevLett.132.076903, which provides the THz-STM setup of the quantum superposition microscope in Sec. I, including Ref. [19]; the calibration of THz pulse in the STM junction in Sec. II, including Refs. [20–22]; the simulation of TIDCS without photon absorption in Sec. III; the density matrix approach of Ramsey fringe in Sec. IV, including Ref. [23]; the analysis of THz-induced DC current signal in Sec. V, including Ref. [24]; and a discussion on the nature of TLS for H_2 in Sec. VI, including Refs. [3,5,9,25–35].

[19] N. T. Yardimci, S. H. Yang, C. W. Berry, and M. Jarrahi, High-power terahertz generation using large-area plasmonic photoconductive emitters, IEEE Trans. Terahertz Sci. Technol. **5**, 223 (2015).

[20] T. L. Cocker, V. Jelic, R. Hillenbrand, and F. A. Hegmann, Nanoscale terahertz scanning probe microscopy, Nat. Photonics **15**, 558 (2021).

[21] G. Czap, P. J. Wagner, F. Xue, L. Gu, J. Li, J. Yao, R. Wu, and W. Ho, Probing and imaging spin interactions with a magnetic single-molecule sensor, Science **364**, 670 (2019).

[22] M. Müller, N. Martín Sabanés, T. Kampfrath, and M. Wolf, Phase-resolved detection of ultrabroadband THz pulses inside a scanning tunneling microscope junction, ACS Photonics **7**, 2046 (2020).

[23] S. Mukamel, *Principles of Nonlinear Optical Spectroscopy* (Oxford University Press, New York, 1995).

[24] D. A. Steck, Quantum and atom optics (2007), available online at http://steck.us/teaching (revision 0.13.10, 22 September 2021).

[25] T. Sugimoto, Y. Kunisada, and K. Fukutani, Inelastic electron tunneling mediated by a molecular quantum rotator, Phys. Rev. B **96**, 241409(R) (2017).

[26] N. D. Lang, Interaction between closed-shell systems and metal surfaces, Phys. Rev. Lett. **46**, 842 (1981).

[27] V. I. Kozub and A. M. Rudin, Zero-bias anomaly of point-contact resistance due to adiabatic electron renormalization of dynamical defects, Phys. Rev. B **55**, 259 (1997).

[28] J. von Delft, D. C. Ralph, R. A. Buhrman, S. K. Upadhyay, R. N. Louie, A. W. W. Ludwig, and V. Ambegaokar, The 2-channel Kondo model: I. Review of experimental evidence for its realization in metal nanoconstrictions, Ann. Phys. (N.Y.) **263**, 1 (1998).

[29] P. Merino, A. Rosławska, C. C. Leon, A. Grewal, C. Große, C. González, K. Kuhnke, and K. Kern, A single hydrogen molecule as an intensity chopper in an electrically driven plasmonic nanocavity, Nano Lett. **19**, 235 (2019).

[30] E. O. Göbel, K. Leo, T. C. Damen, J. Shah, S. Schmitt-Rink, W. Schäfer, J. F. Müller, and K. Köhler, Quantum beats of excitons in quantum wells, Phys. Rev. Lett. **64**, 1801 (1990).

[31] D. M. Meekhof, C. Monroe, B. E. King, W. M. Itano, and D. J. Wineland, Generation of nonclassical motional states of a trapped atom, Phys. Rev. Lett. **76**, 1796 (1996).

[32] R. Hanson, V. V. Dobrovitski, A. E. Feiguin, O. Gywat, and D. D. Awschalom, Coherent dynamics of a single spin interacting with an adjustable spin bath, Science **320**, 352 (2008).

[33] C. Wetli, S. Pal, J. Kroha, K. Kliemt, C. Krellner, O. Stockert, H. V. Löhneysen, and M. Fiebig, Time-resolved collapse and revival of the Kondo state near a quantum phase transition, Nat. Phys. **14**, 1103 (2018).

[34] C.-C. Shu, Q.-Q. Hong, Y. Guo, and N. E. Henriksen, Orientational quantum revivals induced by a single-cycle terahertz pulse, Phys. Rev. A **102**, 063124 (2020).

[35] I. Khanonkin, O. Eyal, J. P. Reithmaier, and G. Eisenstein, Room-temperature coherent revival in an ensemble of quantum dots, Phys. Rev. Res. **3**, 033073 (2021).

[36] F. D. Natterer, F. Patthey, and H. Brune, Quantifying residual hydrogen adsorption in low-temperature STMs, Surf. Sci. **615**, 80 (2013).

[37] F. D. Natterer, F. Patthey, and H. Brune, Distinction of nuclear spin states with the scanning tunneling microscope, Phys. Rev. Lett. **111**, 175303 (2013).

[38] F. D. Natterer, F. Patthey, and H. Brune, Resonant-enhanced spectroscopy of molecular rotations with a scanning tunneling microscope, ACS Nano **8**, 7099 (2014).

[39] A. Halbritter, L. Borda, and A. Zawadowski, Slow two-level systems in point contacts, Adv. Phys. **53**, 939 (2004).

[40] T. L. Cocker, V. Jelic, M. Gupta, S. J. Molesky, J. A. J. Burgess, G. D. L. Reyes, L. V. Titova, Y. Y. Tsui, M. R. Freeman, and F. A. Hegmann, An ultrafast terahertz scanning tunnelling microscope, Nat. Photonics **7**, 620 (2013).

[41] V. Jelic, K. Iwaszczuk, P. H. Nguyen, C. Rathje, G. J. Hornig, H. M. Sharum, J. R. Hoffman, M. R. Freeman, and F. A. Hegmann, Ultrafast terahertz control of extreme tunnel currents through single atoms on a silicon surface, Nat. Phys. **13**, 591 (2017).

[42] S. Chen, W. Shi, and W. Ho, Single-molecule continuous-wave terahertz rectification spectroscopy and microscopy, Nano Lett. **23**, 2915 (2023).

[43] M. Nielsen, Phonons in solid hydrogen and deuterium studied by inelastic coherent neutron scattering, Phys. Rev. B **7**, 1626 (1973).

[44] S. Rolf-Pissarczyk and S. Loth, Atomically resolved dynamics of correlated quantum systems, Staats- und Universitätsbibliothek Hamburg, Ph.D. thesis, 2017.

[45] K. Wang, D. M. Mittleman, N. C. J. v. d. Valk, and P. C. M. Planken, Antenna effects in terahertz apertureless near-field optical microscopy, Appl. Phys. Lett. **85**, 2715 (2004).

[46] K. Yoshioka, I. Katayama, Y. Arashida, A. Ban, Y. Kawada, K. Konishi, H. Takahashi, and J. Takeda, Tailoring single-cycle near field in a tunnel junction with carrier-envelope phase-controlled terahertz electric fields, Nano Lett. **18**, 5198 (2018).

[47] S. Yoshida, H. Hirori, T. Tachizaki, K. Yoshioka, Y. Arashida, Z.-H. Wang, Y. Sanari, O. Takeuchi, Y. Kanemitsu, and H. Shigekawa, Subcycle transient scanning tunneling spectroscopy with visualization of enhanced terahertz near field, ACS Photonics **6**, 1356 (2019).

[48] S. Sheng, A.-C. Oeter, M. Abdo, K. Lichtenberg, M. Hentschel, and S. Loth, Launching coherent acoustic phonon wave packets with local femtosecond Coulomb forces, Phys. Rev. Lett. **129**, 043001 (2022).

[49] L. Novotny and B. Hecht, *Principles of Nano-Optics* (Cambridge University Press, Cambridge, England, 2012).

[50] A. Hellman, Polarization-induced dipole moments of physisorbed H_2, Bull. Am. Phys. Soc. (2023).

[51] L. Wang, D. Bai, Y. Xia, and W. Ho, Electrical manipulation of quantum coherence in a two-level molecular system, Phys. Rev. Lett. **130**, 096201 (2023).